DE GRUYTER
OPEN

Communications in Applied
and Industrial Mathematics
ISSN 2038-0909

Research Article

Commun. Appl. Ind. Math. 8 (1), 2017, 1–22
DOI: 10.1515/caim-2017-0001

A coherent modeling procedure to describe cell activation in biological systems

Marco Scianna[1*], Annachiara Colombi[1]

[1]Department of Mathematical Sciences "G. L. Lagrange", Politecnico di Torino, Corso Duca degli Abruzzi 24, 10129, Torino, Italy

[*]Email address for correspondence: marco.scianna@polito.it

Communicated by Roberto Natalini
Received on 11 28, 2016. Accepted on 02 16, 2017.

Abstract

Biological systems are typically formed by different cell phenotypes, characterized by specific biological properties and behaviors. In particular, cells are able to undergo phenotypic transitions (i.e., activation or differentiation) upon internal or external stimuli. In order to take these phenomena into account, we here propose a modelling framework in which cell ensembles can be described collectively (i.e., through a distributed mass density) or individually (i.e., as a group of pointwise/concentrated particles) according to their biological determinants. A set of suitable rules involving the introduction of a cell shape function then defines a coherent procedure to model cell activation mechanisms, which imply a switch between the two mathematical representations. The theoretical environment describing cell transition is then enriched by including cell migratory dynamics and duplication/apoptotic processes, as well as the kinetics of selected diffusing chemicals influencing the system evolution. Remarkably, our approach provides consistency of the same modeling framework across all types of cell representation, as it is suitable to cope with the often ambiguous translation of individual cell arguments (i.e., cell dimensions and interaction radii) into collective cell descriptions. Biologically relevant numerical realizations are also presented: in particular, they deal with phenotypic transitions within cell colonies and with the growth of a tumor spheroid. These phenomena constitute biological systems particularly suitable to assess the advantages of the proposed model and to analyze the role on cell dynamics both of relevant parameters and of the specific form given to the cell shape function.

Keywords: multiscale modeling, hybrid systems, cell differentiation, cell phenotypic transition, multiscale dynamics.

AMS subject classification: 92B05, 92C05, 92C17

1. Introduction

The evolution of a living system is in general a complex and multi-scale phenomenon involving many different but interconnected processes, that occur at different spatio-temporal levels. In particular, macroscopic dynamics of large cell aggregates and tissues results from microscopic behavior of single component cells, which are able to sense and actively interact with the surrounding environment in a non strictly mechanical manner. This gives rise to entirely different dynamics from those seen in standard systems of inert matter (e.g., fluids, gases), whose particles respond passively to relatively simple physical rules. In this respect, the evolution of a cellular ensemble is not the simple superposition of individual behaviors. In fact, complex interactions arise among cells, leading to the spontaneous emergence of phenomena.

In particular, in a wide range of biological systems, collective cell movement is the principal migration mode and it results from the coexistence and the interactions between multiple cell populations, or between multiple clones of the same population, each having specific functions and migratory properties. For instance, few specialized cells typically behave as a patterning guidance for the unspecialized part of the aggregate [1–3]. Such mechanisms are mainly regulated by temporary activations and/or long-lasting differentiation processes, that define the leader/differentiated individuals within the cell group [4]. Relevant examples of these phenomena include the so-called tip cell selection and lateral inhibition, which establishes the leader endothelial cells during physio-pathological vascularization, a process largely mediated by selected vascular endothelial growth factor (VEGF)-induced delta-notch signaling pathways [5–7], and the epithelial-to-mesenchymal transition (EMT), which is instead typical of different stages of morphogenesis and organogenesis. Similarly, during skin repair after injury, epidermal monolayers invade the wound region moving across two-dimensional extracellular matrix (ECM) substrates, with activated cells located at the front of the population that generate traction forces on the collagenous matrix and are able to synthesize a new basement membrane, whereas the movement of following individuals is only due to cell-cell and cell-matrix adhesive interactions [4]. Typical phenotypic differences are also observed in pathological situations, such as in tumor growth. Nutrient gradients form in fact within a solid cancer mass, causing a well-localized differentiation of malignant cells, which typically differentiate in an outer viable rim of highly metabolic and proliferative individuals and a central quiescent (possibly necrotic) core. In particular, the external cells, which are difficult to be clinically detected, have the greatest potential to metas-

tasize, displaying an evident ability to evade destruction by the immune system enter the host bloodstream or lymphatics, extravasate at a distant site, and establish secondary colonies with devastating consequences for the wellbeing of the patient [8,9].

From a mathematical point of view, it is indeed desirable to develop modelling structures able to capture and represent different cell behaviors as well as the relative mechanisms of cell activation and phenotypic transitions. In this respect, following the idea presented in [10], we here propose an innovative modelling approach, which allows to integrate within the same environment both the dynamics of quiescent cell aggregate, *collectively* described through a proper spatial mass density and the phenomenology of sets of activated individuals, *individually* represented by pointwise/concentrated particles. Further, our mathematical framework includes rules to reproduce cell differentiation by the use of a proper *shape function* which gives the correspondence between the two cell descriptive instances. In order to apply the proposed approach to specific biological problems, the resulting hybrid model is finally enriched with proper equations describing the behavior of each cell clone (i.e., activated/inactivated), including movement and duplication/apoptosis processes, and the kinetics of extracellular chemicals involved in the phenomena of interest.

The remaining part of the article is indeed organized as follows. In Section 2, we present the main model features relative to cell phenotypic transitions, supported in Section 3 by sample test applications that show how the multiscale cell differentiation procedure works. Section 4 is then devoted to introduce possible laws for cell migratory and growth dynamics. Section 5 proposes the application of the model to the avascular invasion of solid tumor, whereas Section 6 finally includes some conclusive remarks as well as comments on the pertinent literature.

2. Mathematical Model I: Cell Phenotypic Transitions

An aggregate of cells within a two dimensional domain $\Omega \subset \mathbb{R}^2$ can be collectively described by defining a spatial mass density distribution $\rho(t, \mathbf{y}) : \mathbb{R}_+ \times \Omega \to \mathbb{R}_+$ such that

$$\int_\Omega \rho(t, \mathbf{y}) d\mathbf{y} = M(t) \quad \forall\, t, \tag{1}$$

where $M(t) \in \mathbb{R}_+$ is the actual mass of the whole cell ensemble. As we will see in the following, ρ can evolve following a balance equation with non local intercellular interactions whereas $M(t)$ can possibly vary in time according to suitable growth/death processes (modeled, for instance, by exponential or logistic laws).

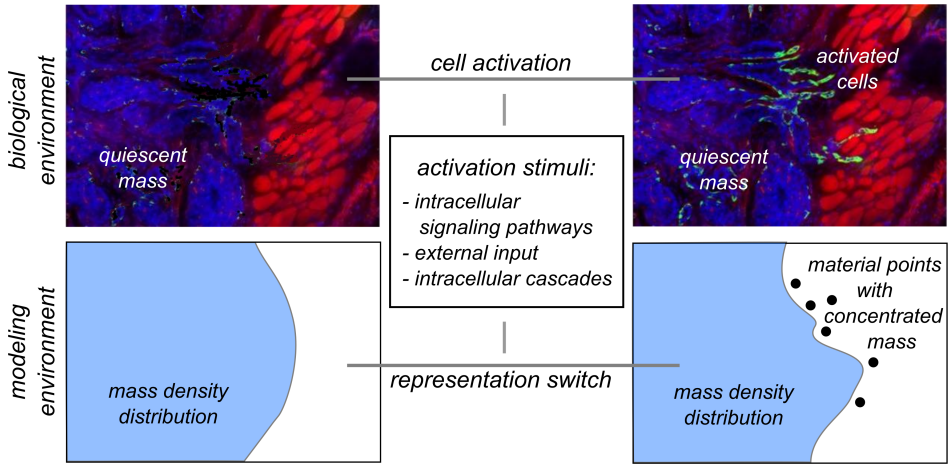

Figure 1. In biological systems, cell activation is triggered both by external stimuli and by intracellular signaling cascades. Such phenotypic transitions can be reproduced in the proposed mathematical framework by a switch between a distributed and a localized cell representation. The former in fact properly gives a collective description of an undifferentiated cell ensemble, the latter is instead particularly adapt to reproduce a set of differentiated cells.

However, in a wide range of biological phenomena, one or few cells are able to undergo phenotypic transitions, which are induced either by intracellular signals or by extracellular stimuli, see Fig. 1. For instance, high enough levels of microenvironmental chemicals can trigger cell *differentiation/activation*. In these cases, the proposed description of the system, based on a collective density, is no longer adapt. The activated cells require in fact a more detailed representation, i.e., with a higher level of individual detail: for instance, they can be more properly regarded as localized material points, with concentrated mass m, which are identified by their exact position in space. It is indeed necessary to define a formal procedure to figure out an individual pointwise description of the differentiated cells from the ensemble representation of the system given by the mass density, as sketched in Fig. 1. In this respect, let us first assume that an input triggers cell activation in a given point $\mathbf{x}_s \in \Omega$ at a given time $t \geq 0$ (s for source): then, as a consequence, a cell differentiates and it is assigned a localized representation, i.e., a material point is added at $\mathbf{x}_s$, while the corresponding mass m has to be removed by the density of the remaining *inactivated* aggregate. Such a decrement in the density ρ can be spatially distributed according to a positive Lebesgue integrable function $w_{\mathbf{x}_s} : \Omega \mapsto \mathbb{R}_+$, centered in $\mathbf{x}_s$ with supp $w_{\mathbf{x}_s} = \mathcal{I}_{\mathbf{x}_s} \subseteq \Omega$. Such a function, that hereafter will

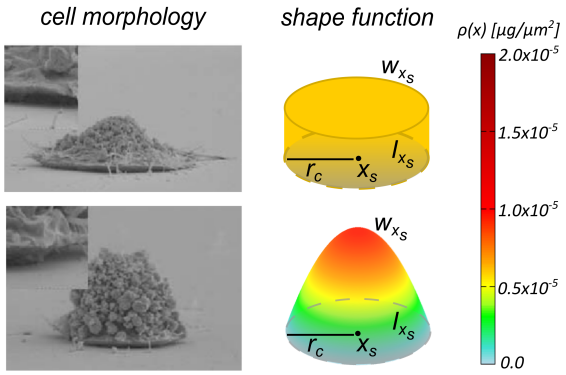

Figure 2. Sample cell morphologies with possible corresponding forms of the shape function introduced in Eq. (2). In particular, the right panels reproduce the shape function $w_{\mathbf{x}_s}$ defined either in Eq. (5) (top) or in Eq. (6) (bottom).

be denoted as *shape function*, has to satisfy the following property

$$\int_{\Omega} w_{\mathbf{x}_s}(\mathbf{y})d\mathbf{y} = m \tag{2}$$

and has units $\mu g/\mu m^2$. Obviously, cell activation, and the relative switch between the two mathematical descriptive instances, is possible only if there is a sufficient amount of mass over the support $\mathcal{I}_{\mathbf{x}_s}$ of $w_{\mathbf{x}_s}$, i.e., if $\rho(t, \mathbf{y}) \geq w_{\mathbf{x}_s}(\mathbf{y})$, $\forall\, \mathbf{y}$ at time t. If this condition is satisfied, the updated cell density is given by

$$\rho(\bar{t}, \mathbf{y}) = \rho(t, \mathbf{y}) - w_{\mathbf{x}_s}(\mathbf{y}) \quad \forall\, \mathbf{y} \in \Omega, \tag{3}$$

whereas, as already explained, at the same time $\bar{t}$, a localized material point "appears" in $\mathbf{x}_s$, giving rise to a *hybrid* description of the system. In this respect, we remark that the activated cell takes places in the barycenter of the shape function and carries the same amount of mass. The notation $\bar{t}$ is used since a cell phenotypic transition can be considered an almost instantaneous phenomenon (with respect to the characteristic times of other cell dynamics) which gives rise to an intermediate system configuration that, in turn, represents the initial condition for the successive evolution of the system.

More in general, if we then extend the above-described procedure in time, or to the case of multiple simultaneous cell differentiations, at any time t, there is the coexistence of a given number, say $N(t)$, of activated individuals, whose distribution will be described hereafter by a vector

$$\mathbf{X}(t) = \{\mathbf{x}_1(t),\ \mathbf{x}_2(t),\ \ldots,\ \mathbf{x}_{N(t)}\}, \tag{4}$$

and of a mass $M(t)$ of an inactivated cell ensemble, defined by its density ρ.

In principle, there exist several possible options to properly explicit the form of the shape function $w_{\mathbf{x}_s}$. In particular, we first assume that the mass of an activated cell has to be accounted within a round region around its position, whose extension is defined, for instance, by a mean cell measure. In this respect, recalling the above-introduced notation, it is consistent to define $\mathcal{I}_{\mathbf{x}_s}$ as a ball centered in $\mathbf{x}_s$, with radius equal to r_c, which obviously depends on the type of cells of interest, see Fig. 2. Further, the decrement in the mass density due to the cell activation can be either uniformly distributed over $\mathcal{I}_{\mathbf{x}_s}$, as in the case of

$$w_{\mathbf{x}_s}(\mathbf{y}) = \begin{cases} \dfrac{m}{\pi r_c^2}, & \text{if } \mathbf{y} \in \mathcal{I}_{\mathbf{x}_s}; \\ 0, & \text{otherwise,} \end{cases} \tag{5}$$

or inhomogeneous in space. In this case, the shape function $w_{\mathbf{x}_s}$ may for example resemble the morphology of cells seeded on planar substrates, accounting therefore of a denser central nuclear region

$$w_{\mathbf{x}_s}(\mathbf{y}) = \begin{cases} \dfrac{4\,m}{\pi\,(r_c)^8}\,(\,r_c^2 - |\mathbf{x}_s - \mathbf{y}|^2\,)^3, & \text{if } \mathbf{y} \in \mathcal{I}_{\mathbf{x}_s}; \\ 0, & \text{otherwise;} \end{cases} \tag{6}$$

where $|\cdot|$ identifies the modulus of a vector in the Euclidean norm. A graphical sketch of the above-introduced forms of the shape function is given in Fig. 2.

3. Numerical Results - I

We now propose two series of numerical tests, designed both to visualize the above-introduced modeling procedure that implements cell activation and to highlight the effects on cell dynamics of different forms given to the shape function introduced in Eq. (2). In particular, we will employ either the form defined in Eq. (5) or the one defined in Eq. (6). However, in both cases, r_c is fixed equal to 15 μm and m to $1.8 \cdot 10^{-3}$ μg, which are values coherent with the mean measures of most eukaryotic cell lineages [11]. Further, in all the following simulations, we will constantly start with an undifferentiated cell aggregate placed in the center of 700 μm $\times$ 700 μm domain Ω, characterized by an inhomogeneous spatial density distribution. In this respect, referring to the hybrid system representation, we will indeed always have that $N(0) = 0$ (i.e., $\mathbf{X}(0) = \emptyset$) and $M(0) = 0.3$ μg.

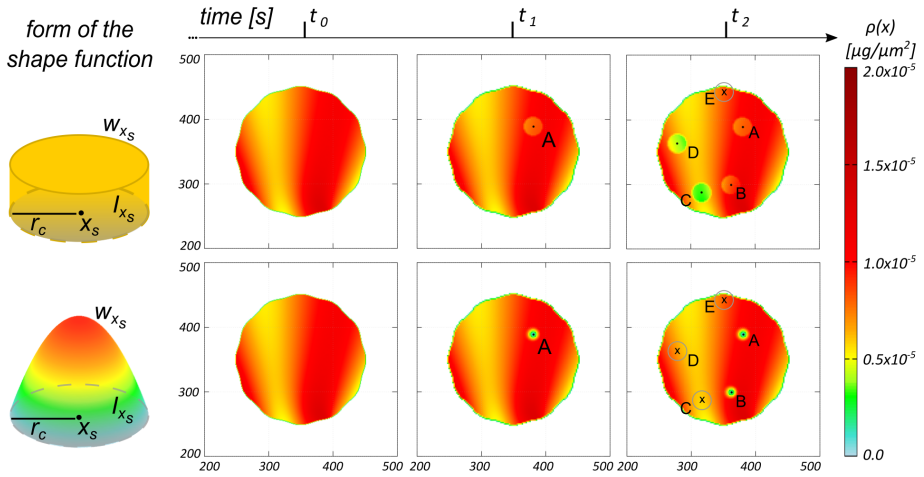

Figure 3. Cell phenotypic activation (with the coherent switch between the corresponding mathematical descriptions) induced at successive instants at selected points within an initially quiescent cell colony. Top panels: Cell dynamics obtained by the use of the shape function given in Eq. (5). Bottom panels: Cell dynamics obtained by the use of the shape function given in Eq. (6). In both cases the initial round cell aggregate is characterized by an inhomogeneous distribution of mass. At t_1, cell activation is proposed and occurs in both settings at point **A**. At t_2, cell differentiation is then induced at points **B**, **C**, **D** and **E**. In the case of the shape function defined in Eq. (5) cell phenotypic transition actually occurs in **B**, **C**, and **D**, whereas in the case of the shape function given in Eq. (6) cell activation is observed only in **B**. In all the other cases, the mass density distributed around the points of interest is in fact not sufficient to give rise to a differentiated individual, given the employed shape function. We remark that, for graphical purposes, in each panel is represented only the central part of the computational domain Ω.

Table 1. Parameter settings used for the simulations in Figs. 3 and 4.

Parameter	Description	Value & Units	Reference(s)
Ω	computational domain	700×700 μm^2	
r_c	cell radius	15 μm	[11]
m	cell mass	$1.8{\cdot}10^{-3}$ μg	[11]
D	chemical diffusion coefficient	10 μm^2/s	[12,13]
ϵ	chemical decay rate	$1.8{\cdot}10^{-4}$ s^{-1}	[12,13]
c_0	chemical production rate	$2.17{\cdot}10^{-4}$ μM	[12,13]
c_s	cell activation chemical threshold	10^{-8} μM	estimated in [10]
R_{inh}	spatial inhibition radius	40 μm	estimated in [10]

In the first set of realizations, cell activation is induced at selected instant times in randomly chosen points within the colony. In particular, at

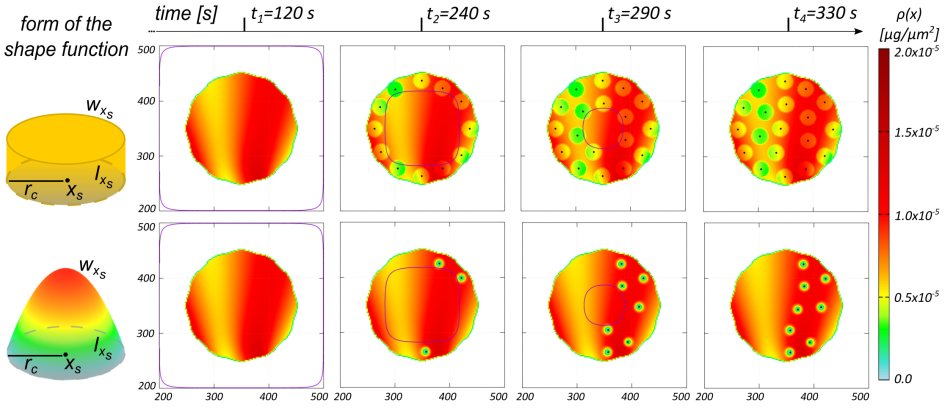

Figure 4. Cell phenotypic activation (with the coherent switch between the corresponding mathematical descriptions) induced by a diffusive chemical factor. The use of the shape function given in Eq. (5) results in consecutive differentiations of radially symmetric rings of cells. On the opposite, the use of the shape function defined in Eq. (6) results in the fact that cell activation only occurs in the densest stripe of the cell aggregate. In both cases, we start with an inhomogeneous undifferentiated colony, whereas in each panel the violet line indicates the concentration of the chemical equal to the activation threshold c_s. We remark that, for graphical purposes, in each panel is represented only the central part of the computational domain Ω.

a given time t_1, cell differentiation is proposed to take place in a single point $\mathbf{A} = (381\ \mu\text{m}, 389\ \mu\text{m})$ within the colony. As it is possible to see in Fig. 3, such a cell phenotypic transition occurs regardless of the specific form assigned to the shape function: in both cases, there is in fact a sufficient amount of distributed mass located over the support of the corresponding $w_{\mathbf{A}}$ (i.e., $\rho(t_1, \mathbf{y}) \geq w_{\mathbf{A}}(\mathbf{y})$, $\forall\ \mathbf{y} \in \Omega$). As a result, in both settings (but with a clearer evidence in the case of the shape function defined in Eq. (5), given its mass distribution), the localized cell formed in $\mathbf{A}$ is surrounded by a round area of radius r_c characterized by a reduction of the local mass density. Successively, at t_2, cell phenotypic transitions are simultaneously proposed to take place in four different locations of the undifferentiated colony (i.e., $\mathbf{B} = (363\ \mu\text{m}, 299\ \mu\text{m})$, $\mathbf{C} = (317\ \mu\text{m}, 287\ \mu\text{m})$, $\mathbf{D} = (279\ \mu\text{m}, 363\ \mu\text{m})$ and $\mathbf{E} = (351\ \mu\text{m}, 441\ \mu\text{m})$). In the case of the use of the shape function given in Eq. (5), cell activation is observed in three points, i.e., $\mathbf{B}$, $\mathbf{C}$ and $\mathbf{D}$ (see Fig. 3, top panel). On the opposite, the use of the shape function given in Eq. (6) allows to have cell differentiation only in $\mathbf{B}$ (see Fig. 3, bottom panel). In each setting, the mass density distributed around the remaining points is in fact not sufficient to constitute a localized

differentiated individual.

In the second set of simulations, cell activation is instead triggered by the activity of a chemical factor, which is assumed to evolve according to the following standard reaction-diffusion equation:

$$(7) \qquad \begin{cases} \dfrac{\partial c}{\partial t}(t,\mathbf{y}) = D\Delta c(t,\mathbf{y}) - \epsilon c(t,\mathbf{y}), & \mathbf{y} \in \Omega; \\ \\ c = c_0, & \mathbf{y} \in \partial\Omega, \end{cases}$$

where D is the constant and homogeneous diffusion coefficient, ϵ is the decay rate, and c_0 indicates a constant production of the molecular substance over the entire boundary of the computational domain Ω. Their specific values, summarized in Table 1, are taken from the experimental literature relative to vascular endothelial growth factor isoforms (VEGFs), which has been widely demonstrated to induce cell activation during physio-pathological vascular progression [12,13]. We set that a minimum concentration threshold, c_s, is needed to locally (i.e., in a given point of the aggregate) promote cell activation. Finally, in order to avoid the formation of quasi or completely overlapped differentiated individuals, we assume that the presence of an activated cell inhibits further phenotypic transitions within a surrounding ball of radius $R_{\text{inh}} = 40$ μm: this modeling rule is the computational counterpart of a wide range of well-known signaling pathways, such as the Delta-Notch regulatory mechanism. The obtained results are reproduced in Fig. 4, where in particular a violet line is a level set that indicates a concentration of the chemical equal to the activation threshold c_s. In the case of the use of the shape function given in Eq. (5) (top panels), we observe consecutive (i.e., form the edge to the bulk of the spheroid) differentiations of two rings of cells, almost radially distributed, until the phenotypic transition of a single individual in the center of the colony. On the opposite, the use of the shape function defined in Eq. (6) results in the fact that cell activation only occurs in the densest stripe of the cell aggregate, despite an analogous chemical field (see Fig. 4, bottom panels). These simulation outcomes further confirm that the choice of the specific form of the shape function w substantially affects the overall model behavior and corresponding dynamics.

4. Mathematical Model II: Cell Growth and Movement

We now enrich the proposed mathematical environment by including proper cell migratory dynamics and proliferation/death processes. In this respect, a key feature of our hybrid modelling framework is the possibility to define a distinct evolution law for the different cell phenotypes forming

the system of interest. Hereafter, we will denote by the superscript "A" the terms relative to the group of activated cells and by the superscript "U" those relative to the undifferentiated mass, whose distribution is given by the density ρ. First of all, it is consistent to use a set of first order ODEs to describe the migration of the activated individuals. The dynamics of the inactivated part of the cell system is instead assumed to be regulated by the local form of a mass balance equation. As graphically sketched in Fig. 5, the evolution of the overall system is therefore defined as it follows

$$\begin{cases} \dfrac{d\mathbf{x}_j(t)}{dt} = \mathbf{v}_{\mathrm{A}}(\mathbf{x}_j(t)), \quad j = 1, \dots, N(t), \\ \\ \dfrac{\partial \rho(t,\mathbf{y})}{\partial t} + \nabla \cdot (\rho(t,\mathbf{y})\ \mathbf{v}_{\mathrm{U}}(t,\mathbf{y})) = \Gamma(t,\mathbf{y}); \end{cases} \tag{8}$$

where $\mathbf{v}_{\mathrm{A}}$ and $\mathbf{v}_{\mathrm{U}}$ are the velocity of the two cell phenotypes, respectively, while the term Γ is the proliferation/apoptosis rate of the distributed part of the aggregate. It is worth to notice that, in Eq. (8), we have assumed that the velocity of moving individuals and not their acceleration is proportional to the sensed forces: this is the so-called *overdamped force-velocity assumption*, that holds for extremely viscous regimes, such as biological environments (see [14] for a detailed comment). On the other hand, we here do not account possible duplication/death processes of activated individuals: however, they can be introduced in the mathematical environment by defining proper evolution laws for their number N and for the location of the newly born individuals.

In general, cell migratory behavior results from the superimposition both of a productive directional locomotion and of dynamics resulting from intercellular interactions. In Eq. (8), it is indeed consistent to set

$$\begin{cases} \mathbf{v}_{\mathrm{A}}(\mathbf{x}_j(t)) = \widehat{\mathbf{v}}_{\mathrm{A}}(\mathbf{x}_j(t)) + \displaystyle\sum_{i=1}^{N} m\ \mathbf{K}^{\mathrm{AA}}(\mathbf{x}_i(t) - \mathbf{x}_j(t)) + \\ \qquad\qquad + \displaystyle\int_{\Omega} \mathbf{K}^{\mathrm{AU}}(\boldsymbol{\xi} - \mathbf{x}_j(t))\rho(t,\boldsymbol{\xi})\, d\boldsymbol{\xi}; \\ \\ \mathbf{v}_{\mathrm{U}}(\mathbf{y}) = \widehat{\mathbf{v}}_{\mathrm{U}}(\mathbf{y}) + \displaystyle\sum_{i=1}^{N} m\ \mathbf{K}^{\mathrm{UA}}(\mathbf{x}_i(t) - \mathbf{y}) + \int_{\Omega} \mathbf{K}^{\mathrm{UU}}(\boldsymbol{\xi} - \mathbf{y})\rho(t,\boldsymbol{\xi})\, d\boldsymbol{\xi}. \end{cases} \tag{9}$$

Specifically, the functions $\widehat{\mathbf{v}}_{\mathrm{A}}, \widehat{\mathbf{v}}_{\mathrm{U}} : \mathbb{R}^2 \mapsto \mathbb{R}^2$ implement the directional contribution to cell velocity, which may arise from environmental determinants, e.g., the local concentration/stiffness of the extracellular matrix

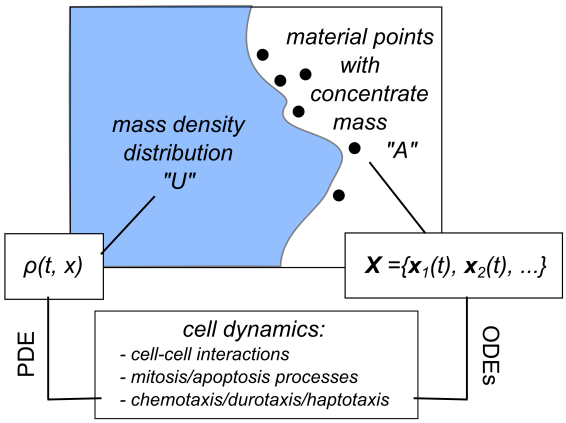

Figure 5. The activation of individual cells within a quiescent aggregate gives rise to a hybrid environment, which is characterized by the coexistence of a group of material points and a spatially distributed mass density. The dynamics of the overall system has indeed to be approached by a coupled-hybrid mathematical framework, where a set of ODEs describes the evolution of the differentiated cells, whereas a balance equation defines the evolution of the undifferentiated rest of the aggregate.

components (haptotaxis/durotaxis) or from the spatial distribution of some diffusive chemicals (chemotaxis). The other terms in Eq. (9) represent instead the velocity components due to direct intercellular interactions. In this respect, the kernels $\mathbf{K}^{\alpha\beta} : \mathbb{R}^2 \mapsto \mathbb{R}^2$ (where $\alpha, \beta, \in \{\text{A, U}\}$) define how a cell element belonging to phenotype α is influenced in its dynamics by a cell element of phenotype β. We indeed have both homotypic (i.e., if $\alpha = \beta$) and heterotypic (i.e., if $\alpha \neq \beta$) intracellular interactions. The specific form of each $\mathbf{K}^{\alpha\beta}$ have then to account for the following set of assumptions:

- intercellular interactions involve cell-cell adhesion, due to the expression of cadherin adhesive molecules, and cell-cell repulsion, which reproduces cell resistance to compression;
- the resulting velocity components give an effect along the direction connecting the interacting elements, depending on their relative distance;
- intercellular interactions are isotropic and metric (i.e., they occur only within limited neighborhoods around the interacting elements).

Similar hypotheses underline intercellular interaction terms introduced in [15] and [16], where a hybrid discrete/continuous representation of two-population systems are obtained by employing a measure-theoretic approach. Other examples of non-local integro-differential models to describe selected dynamics of heterogeneous cell aggregates are proposed in [17], [18]

and [19]. In particular, in [17] and [18], the authors use a continuous approach to model cell adhesion with an integral term over a sensing region, which is defined as the area over which a cell can sense the surrounding environment. In [19], instead, the dynamics of both homogeneous and heterogeneous aggregates are given by a non-local PDE model, which includes both attracting and repelling signals directly transmitted over different interaction ranges.

5. Numerical Results II: Avascular Tumor Growth and Invasion

A solid tumor is typically formed by two clones of malignant cells, that have equal geometrical dimensions but distinct behavior: a differentiated/metastic group of individuals, activated by a given amount of nutrients or growth factors and hereafter labelled by "A", and an undifferentiated quiescent mass, coherently labeled by "U". The former cell phenotype has reduced adhesive interactions and a high migratory ability (in particular, high chemotactic strength). On the contrary, the latter cell clone has significant adhesiveness and enhanced proliferation/death cycles. Taking these considerations into account, it is natural to use a pointwise description for the N_{A} metastatic individuals (whose positions are indeed defined by the vector introduced in Eq. (4)) and a distributed representation for the rest of the tumor mass (defined by the mass density ρ whose integral over the domain gives the total mass M_{U}). The overall hybrid environment evolves following the coupled ODE-PDE system of Eq. (8), with the velocity components defined in Eq. (9). In particular, according to the above biological considerations, we set:

(10)
$$\begin{cases} \widehat{\mathbf{v}}_{\mathrm{A}}(\mathbf{x}_j(t)) = \mathbf{v}_{\mathrm{chem}}(\mathbf{x}_j(t)) = \min\{k_0|\nabla c(t,\mathbf{x}_j(t))|;\ v_{\max}\}\dfrac{\nabla c(t,\mathbf{x}_j(t))}{|\nabla c(t,\mathbf{x}_j(t))|}; \\ \widehat{\mathbf{v}}_{\mathrm{U}}(\mathbf{y}) = 0; \\ \Gamma(t,\mathbf{y}) = \left[\gamma\left(1-\dfrac{\rho(t,\mathbf{y})}{\rho_{\max}}\right)-\delta\right]\rho(t,\mathbf{y})\,H(t-T_\Gamma). \end{cases}$$

Entering in more details, $\mathbf{v}_{\mathrm{chem}}$ is a chemotactic velocity component that, as already seen, is active only for metastatic individuals, as c is the concentration of molecular growth/motility factors, whose kinetics are described in Eq. (7), with the same parameters used in the simulations proposed in Section 3. In particular, c_0 represents a constant supply of chemical substances from the host tissue to the tumor. Further, $k_0 = 4 \cdot 10^9\ \mu\mathrm{m}^2/(\mu\mathrm{Ms})$ is the

chemotactic coefficient while $v_{\max} = 0.018$ μm/s is a maximum admissible speed, taken from the biological literature [11]. Γ gives then a plausible law for growth processes of the quiescent part of the tumor, which start after $T_\Gamma = 2$ hours, as $H(\,\cdot\,)$ is the Heaviside function. In particular, $\gamma = 10^{-3}$ s^{-1} and $\delta = 10^{-4}$ s^{-1} are the proliferation and death rate, respectively, while $\rho_{\max} = 2 \cdot 10^{-5}$ μg/(μm)^2 is a maximum admissible value for the cell mass density. By assuming logistic growth and constant death rate for the quiescent mass, we are including in the model both a contact-inhibition of cell proliferation and a natural cell apoptosis.

There are several possible options to specify the interactions kernels introduced in Eq. (9): in this respect, for all pairs of $\alpha, \beta, \in \{\mathrm{A}, \mathrm{U}\}$), we set

$$\mathcal{K}^{\alpha\beta}(\mathbf{r}) = \begin{cases} -\dfrac{2F_{\mathrm{r}}^{\alpha\beta}|\mathbf{r}|}{d_{\mathrm{r}}} & \text{if } |\mathbf{r}| < \dfrac{d_{\mathrm{r}}}{2}; \\ 2F_{\mathrm{r}}^{\alpha\beta}\left(\dfrac{|\mathbf{r}|}{d_{\mathrm{r}}} - 1\right) & \text{if } \dfrac{d_{\mathrm{r}}}{2} \le |\mathbf{r}| < d_{\mathrm{r}}; \\ -\dfrac{4F_{\mathrm{a}}^{\alpha\beta}}{(d_{\mathrm{a}} - d_{\mathrm{r}})^2}\,(|\mathbf{r}| - d_{\mathrm{r}})\,(|\mathbf{r}| - d_{\mathrm{a}}) & \text{if } d_{\mathrm{r}} \le |\mathbf{r}| < d_{\mathrm{a}}; \\ 0 & \text{otherwise.} \end{cases} \tag{11}$$

Our choice results in the fact that the forces expressed by the interaction kernels depend on the distance between the interacting components (either pointwise individuals or infinitesimal masses) and are directed along the line ideally connecting them. In this respect, from a biological point of view, d_{r} can be interpreted as a mean cell diameter, that determines a minimal space needed by a cell to survive, while d_{a} represents the maximal distance reached by cell mobile adhesive structures: it is indeed consistent to assume $d_{\mathrm{r}} < d_{\mathrm{a}}$, as wandering cells are able to extends membrane protrusions sufficiently far from their main body. On the other hand, the interaction strengths $F_{\mathrm{r}}^{\alpha\beta}$ represent an intrinsic cell resistance to compression, while $F_{\mathrm{a}}^{\alpha\beta}$ give, from a molecular point of view, the amount of expressed and activated adhesive structures that regulates the cell-cell adhesion. It is worth noting that the interaction radii are set to be independent from the specific cell phenotype, whereas the values of interaction forces rely on the type of cells involved. The underlying hypothesis is in fact that the cell subpopulations forming the tumor are two clones of the same cell lineage that have equal physical properties but different behavior. In other words, we are assuming that chemical-induced phenotypic differentiations preserve cell physical dimensions and uniquely determine variations in the

intercellular interaction force components (as well as in the sensitivity to chemotactic cues). In particular, according to experimental measurements on tumors (refer to [20] for gliomas and to [21] for ovarian cancer spheroids), we set $d_{\mathrm{r}} = 30$ μm and $d_{\mathrm{a}} = 60$ μm. The specific values of the intercellular adhesive strengths have been instead empirically estimated, after a number of trial simulations and in accordance with the above-explained considerations, equal to

$$F_{\mathrm{r}}^{\mathrm{AA}} = F_{\mathrm{r}}^{\mathrm{UU}} = 10^{-4} \ \mu\mathrm{m}/(\mu\mathrm{g\,s});$$

$$F_{\mathrm{r}}^{\mathrm{AU}} = F_{\mathrm{r}}^{\mathrm{UA}} = 10^{-5} \ \mu\mathrm{m}/(\mu\mathrm{g\,s});$$

$$F_{\mathrm{a}}^{\mathrm{AA}} = 0 \ \mu\mathrm{m}/(\mu\mathrm{g\,s}); \qquad F_{\mathrm{a}}^{\mathrm{UU}} = 2.5 \cdot 10^{-5} \ \mu\mathrm{m}/(\mu\mathrm{g\,s});$$

$$F_{\mathrm{a}}^{\mathrm{AU}} = 10^{-5} \ \mu\mathrm{m}/(\mu\mathrm{g\,s}); \qquad F_{\mathrm{a}}^{\mathrm{UA}} = 10^{-2} \ \mu\mathrm{m}/(\mu\mathrm{g\,s}).$$

Finally, we assume that cell activation is locally induced by a sufficiently high concentration of chemical growth factors (which, as seen, also behave as chemotactic cues for the already metastatic individuals). In particular, the cell activation threshold is set equal to to $c_{\mathrm{s}} = 10^{-8}$ μM, i.e., a cell phenotypic transition is actually stimulated in any point $\mathbf{x}_{\mathrm{s}}$ within the tumor if $c(t, \mathbf{x}_{\mathrm{s}}) > c_{\mathrm{s}}$. We employ the shape function defined in Eq. (6) with $r_c = 15$ and $m = 1.8 \cdot 10^{-3}$ μg. As in the case of the simulations proposed in Sect. 3, we also assume that a cell activation in $\mathbf{x}_{\mathrm{s}}$ inhibits further cell differentiation over a ball centered in $\mathbf{x}_{\mathrm{s}}$ itself with radius $R_{\mathrm{inh}} = 100$ μm. However, when cell proliferation starts (i.e., at $T_\Gamma = 2$ hours), we assume a concomitantly downregulation of such a spatial inhibition of cell activation: for all $t > T_\Gamma$, R_{inh} in fact decreases to 15 μm, as a consequence of the pathological overgrowth of the quiescent tumor mass. A summary of the parameter setting is given in Table 2.

Given a domain $\Omega = [0, 700] \times [0, 700]$ μm^2, we start with a completely quiescent tumor spheroid (i.e., $\mathbf{X}(0) = \emptyset$ and $N(0) = 0$), whose mass density is inhomogeneously distributed over a round compact of radius 100 μm to have an overall amount of $M(0) = 0.3$ μg, as reproduced in Fig. 6 (top-left panel). Due to inner interactions, the tumor initially adjusts toward a stable configuration, until the chemical diffusive front reaches the spheroid and locally exceeds the critical threshold of c_{s}. Suddenly, a differentiation (with the corresponding switch in the mathematical descriptive instances) occurs in the most dense part of the malignant mass: in particular, two cells activates, whose distance satisfies the above-described mechanism of spatial inhibition of differentiation. As reproduced in Fig. 6 (top panels), the

Table 2. Parameter setting used for the simulation in Fig. 6.

Parameter	Description	Value & Units	Reference(s)
Ω	computational domain	700×700 μm^2	
r_c	cell radius	15 μm	[11]
m	cell mass	$1.8{\cdot}10^{-3}$ μg	[11]
D	chemical diffusion coefficient	10 μm^2/s	[12,13]
ϵ	chemical decay rate	$1.8{\cdot}10^{-4}$ s^{-1}	[12,13]
c_0	chemical production rate	$2.17{\cdot}10^{-4}$ μM	[12,13]
c_{s}	chemical threshold for cell activation	10^{-8} μM	estimated in [10]
R_{inh}	spatial inhibition radius	100 / 15 μm	estimated in [10]
k_0	chemotactic coefficient	$4{\cdot}10^{9}$ μm^2/(μM s)	estimated in [10]
$v_{\max}$	maximal cell speed	0.018 μm/s	[11]
γ	cell proliferation rate	10^{-3} s^{-1}	estimated in [10]
δ	cell death rate	10^{-4} s^{-1}	estimated in [10]
ρ_{max}	maximum admissible value for cell mass density	$2{\cdot}10^{-5}$ μg/μm^2	estimated in [10]
T_Γ	delay of proliferation/death processes	2 hours	estimated with preliminary simulations
d_r	intercellular repulsion radius	30 μm	[20,21]
d_a	intercellular adhesion radius	60 μm	[20,21]
F_r^{AA}	homotypic repulsion strength between activated cells	10^{-4} μm/μg	estimated in [10]
F_r^{UU}	homotypic repulsion strength within the inactivated mass	10^{-4} μm/μg	estimated in [10]
F_r^{AU}	heterotypic repulsion strength	10^{-5} μm/μg	estimated in [10]
F_r^{UA}	heterotypic repulsion strength	10^{-5} μm/μg	estimated in [10]
F_a^{AA}	homotypic adhesion strength between activated cells	0 μm/μg	estimated in [10]
F_a^{UU}	homotypic adhesion strength within the inactivated mass	$2.5{\cdot}10^{-5}$ μm/μg	estimated in [10]
F_a^{AU}	heterotypic adhesion strength	10^{-5} μm/μg	estimated in [10]
F_a^{UA}	heterotypic adhesion strength	10^{-2} μm/μg	estimated in [10]

activated malignant individuals then chemotactically react to the molecular substance gradient, thereby starting to crawl in the extracellular host toward the nearest edge of the domain. Due to heterotypic adhesive interactions, finger structures, formed by inactivated individuals, extend from the external rim of the tumor mass beside each leader individual. The elongation of malignant cellular tongues is obtained under the assumption that such a first step of tumor infiltration is characterized by mass preservation. In this respect, the collective patterning is uniquely a consequence of cell differentiation and of selected interactions between leader/activated cells

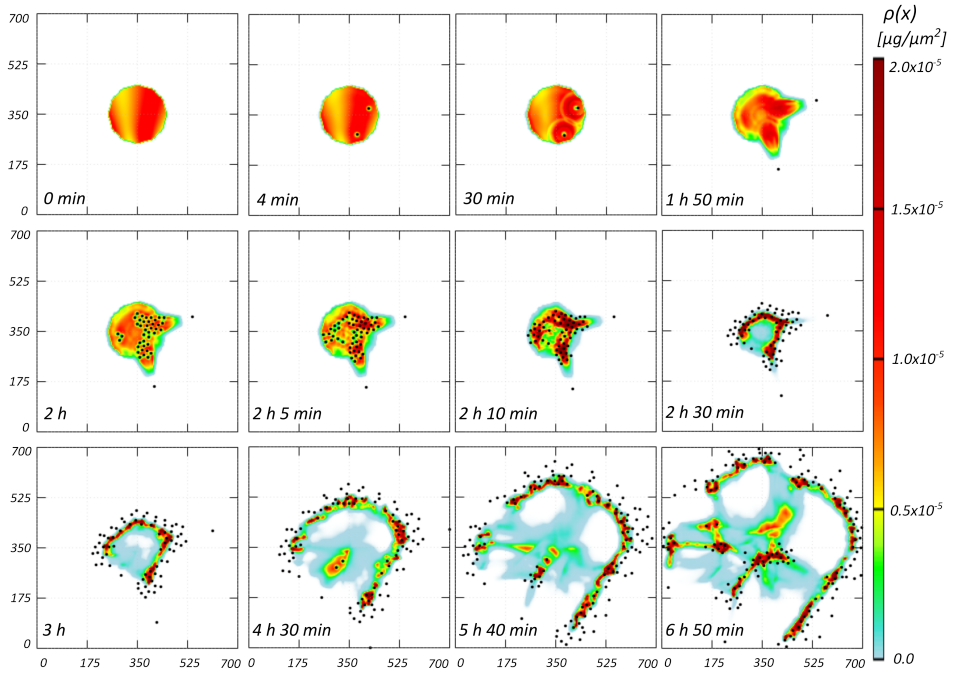

Figure 6. Avascular growth of a tumor spheroid. In the first stage, two single cells differentiate due to the extracellular chemical stimulus. Then, they start to invade the host tissue, followed by finger-like structures emerging from the quiescent malignant mass (top panels). In a second phase (i.e., after 2 hours), cell proliferation starts, resulting in a dramatic enhancement of tumor mass and pathological phenotypic transitions, as a number of cells metastasize (middle panels). Finally, the remaining quiescent mass clusters around the nearest activated cell, thereby forming an invading rim of tumor that expands in the host. The bulk of the original spheroid, which has remained almost deprived of cells, continues instead to proliferate, thereby becoming a source for a possible in situ tumor relapse (bottom panels).

and follower/quiescent individuals. In this respect, it is useful to notice that fingering dynamics arise only from specific ranges of model parameters: too low heterotypic adhesiveness (as well as high enough values of the chemotactic strength) would result in the dispersion of activated cells; on the opposite, a too high exogenous adhesiveness (as well as too low chemotactic response) would result in the absorption of the differentiated individuals within the bulk of the tumor. In the second stage of tumor invasion (i.e., when $t > T_{\Gamma}$, see Fig. 6 (middle panels)), the inclusion both of cell proliferation and of the relaxation of the spatial regulatory mechanism of cell differentiation results in a significant growth of tumor mass and in the consequent dramatic activation of a number of aggressive cells within the

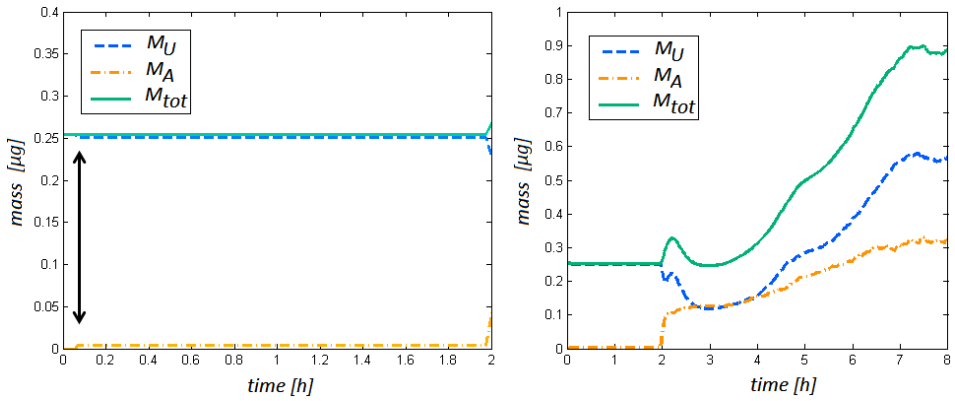

Figure 7. Evolution in time of the mass of the quiescent part of the tumor (i.e., $M_{\mathrm{U}}(t) = \int_\Omega \rho(t,\mathbf{y})d\mathbf{y}$), of the activated individuals (i.e., $M_{\mathrm{A}}(t) = mN_{\mathrm{A}}(t)$), and of the entire disease (i.e., $M_{\mathrm{tot}}(t) = M_{\mathrm{U}}(t) + M_{\mathrm{A}}(t)$). In particular, in the left panel, we plot a zoom view of the first 2 hours of the disease development. The black arrow indicate the chemical-induced activation of the first pair of malignant cells.

most dense parts of the spheroid as well as along the finger structures. The newly differentiated individuals, being characterized by reduced adhesive interactions and increased chemotactic movement, indeed dissociate and spread away. Concomitantly, the remaining quiescent mass tends to cluster around the nearest activated cells. As a result, we observe an invading rim of tumor that expands in the host. On the contrary, the bulk of the original spheroid is almost deprived of cells. However, such a reduced quiescent malignant core goes on proliferating (and possibly differentiating), thereby constituting a source for a further in situ tumor relapse (see Fig. 6 (bottom panels)).

The plots in Fig. 7 describe the time-evolution of the mass of the quiescent part of the tumor (i.e., $M_{\mathrm{U}}(t) = \int_\Omega \rho(t,\mathbf{y})d\mathbf{y}$), of the activated individuals (i.e., $M_{\mathrm{A}}(t) = mN_{\mathrm{A}}(t)$), and of the entire disease (i.e., $M_{\mathrm{tot}}(t) = M_{\mathrm{U}}(t) + M_{\mathrm{A}}(t)$). As it is possible to see in the left graph, until $\approx$ 15 minutes the overall mass of the cancer is constant and equal to the one of its inactivated part. Then two cells differentiate, due to the fact that the chemical front reaches the spheroid edge: as a result, M_{U} slightly decreases and while M_{A} simultaneously increases at the same rate (see the black arrow in the same panel). However, M_{tot} does not vary since there is only a mass exchange between the two malignant subpopulations. At $\approx$ 2 hours, the spatial regulatory mechanism of cell activation is downregulated and the quiescent cell proliferation enters the picture: as a consequence, M_{tot} starts increasing at almost the same rate of M_{U} (right graph in Fig.

7). In particular, the decrements of the quiescent cellular fraction due to cell differentiation are overcome by its growth due to the term at the right hand side of Eq. (8) (and explicitly defined in (10)). In this respect, we can conclude that the observed variations of M_{tot} completely rely on the mitotic/apoptotic processes of the inactivated tumor fraction since, as already explained, cancer cell phenotypic transitions do not affect the overall mass of disease.

It is finally useful to remark that the evolution of the malignant mass captured in our simulations reproduces only the avascular stage of tumor growth (i.e., before the angiogenic transition necessary for the disease to go on survive).

6. Conclusions

A wide range of relevant biological systems is characterized by the coexistence of distinct clones of the same cell lineage, which have specific functions and migratory determinants. Furthermore, in such systems, cells are able to change their phenotype. For instance, in vasculogenesis, tumor growth and invasion, as well as in organogenesis and morphogenesis, relevant component processes result in fact from the specialization of few cells, that are able to activate and behave as a pattern guidance for the remaining part of the system.

In this respect, we here propose a modelling framework where cells within an aggregate can be described either individually, i.e., as a set of localized particles, or collectively, i.e., through a mass density distribution, according to their biological behavior. In particular, our modeling framework defines a coherent procedure to reproduce cell activation via the use of a proper shape function. The proposed theoretical model also includes cell migratory dynamics and interactions, as well as growth mechanisms. The evolution of molecular substances, which possibly influence both cell motility and phenotypic differentiation, are taken in account as well. A first set of illustrative simulations presented in the paper focuses on cell phenotypic transitions within a quiescent aggregate both randomly induced and activated by a diffusive chemical morphogen. Such numerical tests also show nontrivial consequences on cell dynamics of the specific form assigned to the shape function. The proposed modeling approach is then applied to describe the avascular growth and invasion of a tumor mass, which is composed of two cell phenotypes: a set of aggressive activated cells (represented by a pointwise mathematical description) and a quiescent mass (represented by a distributed density). As a result, our simulation environment is able to reproduce the extension of tumor tongues and the subsequent spreading of

metastasis. In this respect, we can observe that the theoretical approach described in this work is particularly suited to deal with problems in which the interplay between different types of mathematical description can be linked to the coexistence of multiple cell populations. In these cases, it is in fact necessary to treat each set of individuals at a distinct scale according to its intrinsic properties.

It is useful to remark that tumor cell activation is here assumed to be triggered by a generic growth/motility factor which, as seen, behaves also as a chemotactic cue for metastatic individuals. As defined in Eq. (7), such a molecular substance is constantly produced at the domain borders, homogeneously diffuses and undergoes a natural decay. The proposed molecular dynamics are reasonable in the case of morphogens such as VEGF isoforms or HGF, which have been provided to be able to activate and guide the migration of cells also within extended colonies [22,23], in agreement with our simulations. A more realistic tumor model would account also for chemical nutrients, such as oxygen and glucose. The kinetics of these types of substances should be described by a reaction-diffusion equation similar to (7), which however should include a cell uptaken term (e.g., $\kappa\rho$, where κ is an internalization rate). As a result, we would observe the emergence of nutrient gradient within the tumor mass: the molecular concentration would be in fact higher at the spheroid edge (i.e., where cell density is lower) and lower in the bulk of the aggregate (i.e., where cell density is higher). In this case, if a nutrient-dependent proliferation rate is added as well, the tumor would differentiate in a central hypoxic/necrotic core and a external ring of highly metabolic cells, which would then constitute the only subpopulation able to sense the presence of growth/motility factors and therefore to activate [24]. In the case of nutrient substances, a further possible model option to create chemical gradients within the tumor would be also the assumption of non-linear diffusion, which is widely used in the field of porous media.

Final remarks and future model developments. For the reasons cited along the text, we expect our method to give an interesting contribution in the development of multiscale approaches to the modeling of cell phenomena. However, the presented mathematical framework has still some important limitations, whose improvements would represent relevant modeling refinements. First, in most of the proposed sets of simulations cell activation occurs when two conditions are satisfied: (i) the concentration of the chemical locally (i.e., at $\mathbf{x}_\mathrm{s}$) exceeds a given threshold and (ii) there is enough cell mass around that point (i.e., over $\mathcal{I}_{\mathbf{x}_\mathrm{s}}$). These assumptions are reasonable from a biological point of view, since most intracellular pathways are

affected by the local presence (and amount) of the molecular substance of interest (e.g., at a given membrane receptor). However, the use of a local thresholding control for cell differentiation may lead to discrepancies between different computer-based realizations (i.e., in the exact location of cell differentiation). They depend from the presence of an artificial/numerical diffusion which is in turn related to the computational method, time step and characteristic grid size used to solve Eq. (7). In this respect, it would be useful to perform a detailed study on how to reduce such numerical artifacts. On the other hand, some other non-local rules for cell activation could be considered (e.g., a control of the chemical amount over a given neighborhood of $\mathbf{x}_s$, maybe over $\mathcal{I}_{\mathbf{x}_s}$ itself). However, such regulatory mechanisms, and underlying assumptions, should be carefully validated by experimental evidence.

Then, some parameters have a poor correspondence with experimentally measurable quantities, although they can be estimated through reasonable biological considerations. This issue may be addressed by implementing different types of interaction kernels. It would be also interesting to describe in more details cell interactions with the extracellular environment, for example mechanical tensions and stresses with the substrate. Further, more sophisticated boundary conditions may be needed in the case of applications dealing with more realistic domains (i.e., analysis of blood flows, collective cell migration in three-dimensional matrix scaffolds, organogenesis). In this respect, a model implementation to three-dimensional environments would be useful as well: however, such an extension would require the definition of different types of shape functions. Future work developments will involve an in-depth analysis of the model stability with respect both to the parameter settings and to the specific choice of the form of the shape function. Further, after a renormalization with respect to the single cell mass, both the density ρ and the discrete variables describing activated individuals can be understood as the probability measure linked to cell positions. In this way, the proposed approach can be interpreted as a probabilistic framework, which is conceptually suited to deal with a statistical characterization of the evolution of biological systems. Finally, in order to further assess the advantages of the proposed modelling framework, it will be interesting to apply the model to other biological problems whose evolution is characterized by cell phenotypic differentiations that preserve cell biophysical properties but lead to different behaviors.

REFERENCES

1. O. Ilina and P. Friedl, Mechanisms of collective cell migration at a glance, *J. Cell. Sci.*, vol. 122, pp. 3203–3208, 2009.
2. A. A. Khalil and P. Friedl, Determinants of leader cells in collective cell migration, *Integr. Biol.*, vol. 2, pp. 568–574, 2010.
3. V. T. Boekhorst, L. Preziosi, and P. Friedl, Plastiticy of cell migration in vivo and in silico, *Annu. Rev. Cell Dev. Biol.*, vol. 32, pp. 491–526, 2016.
4. P. Friedl and D. Gilmour, Collective cell migration in morphogenesis, regeneration and cancer, *Nat. Rev. Mol. Cell. Biol.*, vol. 10, pp. 445–457, 2009.
5. Z. J. Liu, T. Shirakawa, Y. Li, A. Soma, M. Oka, G. P. Dotto, R. M. Fairman, O. C. Velazquez, and M. Herlyn, Regulation of notch1 and dll4 by vascular endothelial growth factor in arterial endothelial cells: implications for modulating arteriogenesis and angiogenesis, *Mol. Cell. Biol.*, vol. 23, pp. 14–25, 2003.
6. M. Scianna, E. Bassino, and L. Munaron, A cellular potts model analyzing differentiated cell behavior during in vivo vascularization of a hypoxic tissue, *Comput. Biol. Med.*, vol. 63, pp. 143–156, 2015.
7. M. Scianna, C. G. Bell, and L. Preziosi, A review of mathematical models for the formation of vascular networks, *J. Theor. Biol.*, vol. 333, pp. 174–209, 2013.
8. K. M. Burleson, M. P. Boente, S. E. Parmabuccian, and A. P. Skubitz, Disaggregation and invasion of ovarian carcinoma ascites spheroids, *J. Transl. Med.*, vol. 4, pp. 1–16, 2006.
9. K. Shield, M. L. Ackland, N. Ahnmed, and G. E. Rice, Multicellular spheroids in ovarian cancer metastases: biology and pathology, *Gynec. Oncol.*, vol. 113, pp. 143–148, 2008.
10. A. Colombi, M. Scianna, and L. Preziosi, Coherent modelling switch between pointwise and distributed representations of cell aggregates, *J. Math. Biol.*, 2016, in press. doi: 10.1007/s00285-016-1042-0.
11. B. Alberts, A. Johnson, J. Lewis, M. Raff, K. Roberts, and P. Walter, *Molecular Biology of the Cell, 4th ed.* Garland Science, 2002.
12. P. Carmeliet and R. K. Jain, Angiogenesis in cancer and other diseases, *Nature*, vol. 407, pp. 249–257, 2000.
13. P. Carmeliet, Angiogenesis in life, disease and medicine, *Nature*, vol. 438, pp. 932–936, 2005.
14. M. Scianna and L. Preziosi, Multiscale developments of cellular potts models, *Mult. Model. Sim.*, vol. 10, pp. 342–382, 2012.
15. A. Colombi, M. Scianna, and A. Tosin, Differentiated cell behavior: a

multiscale approach using measure theory, *J. Math. Biol.*, 2015, in press. doi: 10.1007/s00285-014-0846-z.

16. A. Colombi, M. Scianna, and L. Preziosi, A measure-theoretic model for collective cell migration and aggregation, *Math. Model. Nat. Phenom.*, vol. 1, no. 10, pp. 32–63, 2015.
17. N. J. Armstrong, K. Painter, and J. A. Sherratt, A continuum approach to modelling cell-cell adhesion, *J. Theor. Biol.*, vol. 243, pp. 98–113, 2006.
18. N. J. Armstrong, K. Painter, and J. A. Sherratt, Adding adhesion to a chemical signaling model for somite formation, *Bull. Math. Biol.*, vol. 71, pp. 1–24, 2009.
19. K. J. Painter, J. M. Bloomfield, J. A. Sherratt, and A. Gerisch, A nonlocal model for contact attraction and repulsion in heterogeneous cell populations, *Bull. Math. Biol.*, vol. 77, no. 2, pp. 1132–1165, 2015.
20. H. S. Bell, I. R. Whittle, M. Walker, H. A. Leaver, and S. B. Wharton, The development of necrosis and apoptosis in glioma: experimental findings using spheroid culture systems, *Neuropathol. Appl. Neurobiol.*, vol. 27, pp. 291–304, 2001.
21. M. L. Puiffe, C. L. Page, A. Filali-Mouhim, M. Zietarska, V. Ouellet, P. N. Toniny, M. Chevrette, D. M. Provencher, and A. M. Mes-Masson, Characterization of ovarian cancer ascites on cell invasion, proliferation, spheroid formation, and gene expression in an in vitro model of epithelial ovarian cancer, *Neoplasia*, vol. 9, pp. 820–829, 2007.
22. A. D. Luca, N. Arena, L. M. Sena, and E. Medico, Met overexpression confers hgf-dependent invasive phenotype to human thyroid carcinoma cells in vitro, *J. Cell. Physiol.*, vol. 180, no. 3, pp. 365–371, 1999.
23. M. F. D. Renzo, M. Oliviero, R. P. Narsimhan, S. Bretti, S. Giordano, E. Medico, P. Gaglia, P. Zara, and P. M. Comoglio, Expression of the met/hgf receptor in normal and neoplastic human tissues, *Oncogene*, vol. 6, pp. 1997–2003, 1991.
24. J. M. Brown, Tumor microenvironment and the response to anticancer therapy, *Cancer Biol. Ther.*, vol. 1, pp. 453–458, 2002.